PHYSICAL REVIEW A **89**, 013403 (2014)

Photo-double-ionization of ethylene and acetylene near threshold

B. Gaire,[1] S. Y. Lee,[1] D. J. Haxton,[2] P. M. Pelz,[1] I. Bocharova,[1] F. P. Sturm,[1,3] N. Gehrken,[1,3] M. Honig,[3] M. Pitzer,[3] D. Metz,[3] H.-K. Kim,[3] M. Schöffler,[3] R. Dörner,[3] H. Gassert,[3] S. Zeller,[3] J. Voigtsberger,[3] W. Cao,[4] M. Zohrabi,[4] J. Williams,[5] A. Gatton,[5] D. Reedy,[5] C. Nook,[5] Thomas Müller,[6] A. L. Landers,[5] C. L. Cocke,[4] I. Ben-Itzhak,[4] T. Jahnke,[3] A. Belkacem,[1] and Th. Weber[1]

[1]*Chemical Sciences Division, Lawrence Berkeley National Laboratory, Berkeley, California 94720, USA*

[2]*Chemical Sciences Division and Ultrafast X-Ray Science Laboratory, Lawrence Berkeley National Laboratory, Berkeley, California 94720, USA*

[3]*Institut für Kernphysik, Goethe-Universität, Max-von-Laue-Straße 1, 60438 Frankfurt am Main, Germany*

[4]*J.R. Macdonald Laboratory, Department of Physics, Kansas State University, Manhattan, Kansas 66506, USA*

[5]*Department of Physics, Auburn University, Alabama 36849, USA*

[6]*Institute of Advancend Simulation, Jülich Supercomputer Centre, Forschungszentrum Jülich, D-52425 Jülich, Germany*

(Received 12 November 2013; published 13 January 2014)

We present kinematically complete measurements of the photo-double-ionization of ethylene (double CC bond) and acetylene (triple CC bond) hydrocarbons just above the double-ionization threshold. We discuss the results in terms of the coincident kinetic energy of the photoelectrons and the nuclear kinetic-energy release of the recoiling ions. We have incorporated quantum chemistry calculations to interpret which of the electronic states of the dication have been populated and trace the various subsequent fragmentation channels. We suggest pathways that involve the electronic ground and excited states of the precursor ethylene dication and explore the strong influence of the conical intersections between the different electronic states. The nondissociative ionization yield is small in ethylene and high in acetylene when compared with the dissociative ionization channels. The reason for such a striking difference is explained in part on the basis of a propensity rule that influences the population of states in the photo-double-ionization of a centrosymmetric closed-shell molecule by favoring singlet ungerade and triplet gerade final states. This propensity rule and the calculated potential-energy surfaces clarify a picture of the dynamics leading to the observed dication dissociation products.

DOI: 10.1103/PhysRevA.89.013403 PACS number(s): 33.80.Eh, 33.90.+h

I. INTRODUCTION

In the photo-double-ionization (PDI) of a target atom or a molecule, one photon is absorbed by a single electron, which then interacts with another electron, ejecting both into the continuum and producing one or more charged recoil ions. The essential interaction of the two electrons makes PDI an ideal process for studying electron-electron correlation. Moreover, fragmentation dynamics can be investigated by connecting electronic states to different dissociation channels. In past years, PDI has seen extensive study on two-electron systems such as H_2 and He with intrashell electron-electron correlation and on many-electron diatomic molecules with both intrashell and intershell electron-electron interactions (see, e.g., Refs. [1–5]). The natural next step is to use polyatomic molecular targets to explore the effects of chemical bonding on electron-electron correlation. The PDI of these targets also offers a variety of avoided crossings and conical intersections of potential-energy surfaces (PESs) that produce a rich array of nuclear dynamics during dissociation.

We chose to study closed-shell hydrocarbon molecules with different types of hybridization of their carbon-carbon bond, namely, ethylene (C_2H_4) and acetylene (C_2H_2). We expect the PDI of these two species to be different because of their dissimilar geometries and electronic configurations. The double ionization of these molecules with photon and particle impact has been explored thoroughly in the past in both theory and experiment (ethylene [6–8] and acetylene [9–16]). Previous studies in ethylene include methods such as double-charge-transfer spectroscopy [7,17,18], charge-stripping-mass spectroscopy [19,20], Auger spectroscopy [21,22], and time-of-flight mass spectrometry [23–25]. In all these experiments the detection of the doubly charged ion $C_2H_4^{2+}$ is elusive. This is due to the fact that the time of flight (TOF) of the molecular dication and the fragment ions from other breakup channels overlap. The fragmentation pathways remain unidentified in these studies and a more sensitive probe is needed to pinpoint the existence of a stable dication in the direct PDI near threshold.

Here we utilize a method that allows the coincidence detection of both electrons and the recoil ions produced by double ionization. We choose photon energies close to the PDI threshold where deviations from the Wannier law are expected to be small. By detecting the energies of all particles simultaneously we are able to verify that most electrons are emitted via direct double ionization and that any competing two-step processes such as autoionization or Auger decay play a minor role. This enables the kinematically complete study of the direct PDI of these molecules. We are searching for answers to basic questions. Can the metastable dications of ethylene and acetylene be observed in our measurements? What are the pathways leading to the formation of such dications and competing fragmentation channels? We aim to identify the states that result from the removal of two intrashell electrons and/or two intershell electrons and the role of these states in the subsequent fragmentation process after PDI. For this investigation it is essential to know the PESs of the dications in order to shed light on the ionization and fragmentation mechanisms at work. We have performed calculations of

the excited-state dication potential-energy surfaces, which allow us to identify the states involved by comparison with our measured kinetic energies of the electrons and fragment ions. We also find the dominant ionization channels based on branching ratios.

We present a brief description of the experimental and theoretical methods in the next two sections. The results and discussion follow, beginning with the nondissociative ionization of ethylene molecules.

II. EXPERIMENTAL METHOD

We used cold target recoil ion momentum spectroscopy (COLTRIMS) [26] and performed kinematically complete measurements on the PDI of single ethylene and acetylene molecules. In the COLTRIMS method the target molecules are cooled in a supersonic gas jet and crossed with the photon beam inside a three-dimensional momentum-imaging spectrometer. Our experimental approach is to use photons with energies just above the double-ionization threshold and measure the recoil ions resulting from both nondissociative ionization (NDI) and dissociative ionization (DI) in coincidence with the photoelectrons. Details on the experimental setup and the data collection as well as the analysis schemes can be found in Ref. [27]. We give only a brief description here.

Linearly polarized photons of energies above threshold are provided by beamline 10.0.1 of the Advanced Light Source at Lawrence Berkeley National Laboratory. The ions and electrons generated from the ionization of a single molecule are guided by the static electric field inside the spectrometer to their respective time and position sensitive detectors (located in opposite arms of the spectrometer). A magnetic field parallel to the electric field prevents the energetic electrons from leaving the spectrometer. A collection angle of 4π is achieved for both the recoil ions and electrons (up to a kinetic energy of 15 eV) by using a static electric field of 5.8 V/cm and a magnetic field of 7.1 G. The measured time and position of the ions and electrons are recorded for each event and later used for offline analysis. The TOF and position data are used to construct the full three-dimensional momentum vector of all the collected particles, thereby recording the complete kinematics of the breakup process. Our electron detector has a delay line hex anode for position readout. The redundant position information from the hex anode is very helpful in minimizing losses from the detector dead time, i.e., the ability to detect two electrons arriving at the detector within less than 8 ns and 9 mm apart.

The kinetic energies and angular distributions of the photoelectrons provide information that helps to determine the orbitals from which they were ionized. In this work, however, we focus on the energy distributions only. The photon energy, used in the PDI (i.e., removing two valence electrons in the photoionization), from beamline 10.0.1 of the Advanced Light Source has an uncertainty of less than 0.1 eV. The electron kinetic energy is calibrated using single ionization of helium and the typical error is less than 0.2 eV. The recoil ion kinetic energy is calibrated using the double ionization of N_2 and compared to the kinetic-energy release (KER) distribution in Ref. [28]. The error in our KER measurements is less than ± 0.2 eV. Based on the principle

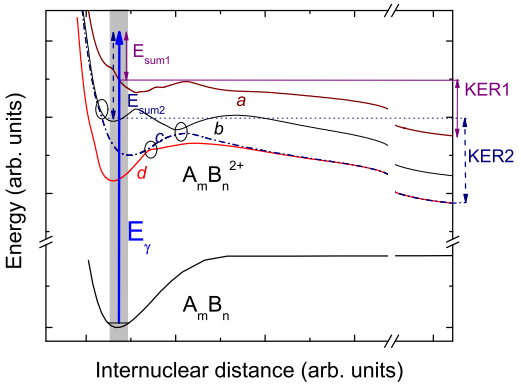

FIG. 1. (Color online) Schematic representation of the photo-double-ionization of a typical A_mB_n molecule. Two pathways are considered as an example. One involves the highly excited potential-energy curve (labeled a) that is dissociative in the given coordinate. The ionization of electrons from this state results in the sum kinetic energy of two electrons (E_{sum1}) and the corresponding kinetic-energy release (KER1) of the fragments. The horizontal line represents the vertical energy, i.e., $E_\gamma - E_{\mathrm{sum1}}$. In a similar way, the second pathway involves a state (labeled b with vertical energy $E_\gamma - E_{\mathrm{sum2}}$) that is nondissociative in this coordinate but is coupled with another state (labeled c) via a conical intersection for instance. Since state c is dissociative the molecule fragments. The KER2 is associated with the asymptotic limit of state c (not b) as the dissociating population transfers from state b to state c (which in fact is also coupled to another state d with the same asymptotic limit). This shows that the dissociation pathways in polyatomic molecules are more complex compared to diatomic molecules since these pathways involve nonadiabatic couplings such as conical intersections and avoided crossings (marked with circles). The shaded vertical area indicates the Franck-Condon region for the given coordinate of the molecule.

of energy conservation, the sum of the kinetic energies of the two ejected electrons (denoted as E_{sum}) subtracted from the photon energy E_γ provides the vertical energy E_{vert} of the state that has been populated by the ionization, i.e., the energy of the precursor dication. This is shown schematically in Fig. 1 for a typical A_mB_n molecule involving two different pathways. The KER is the difference between the energies at which the dissociation begins on the PES and the asymptotic limit of that respective state (see Fig. 1). The states with the right values of vertical energy and KER are considered to represent the most likely pathways in the dissociation process.

The probability to populate a given electronic state of the dication depends mainly on the following factors: available photon energy, the symmetries of the molecule and the emitted electrons, and the overlap between the vibrational wave function of the electronic state of the neutral and those of the dication (i.e., the Franck-Condon factor). For polyatomic molecules, the Franck-Condon factor is evaluated from the multidimensional overlap integrals [29]. Symmetry considerations often result in selection rules for electronic transitions. For example, the valence electron ionization of a centrosymmetric molecule favors the singlet ungerade and triplet gerade states [5,30,31]. In the case of PDI of atomic targets the symmetry of the wave function of the two escaping

TABLE I. Parameters of quantum chemistry calculations.

		Orbitals		No. of configurations		MCSCF weights		
Species	Channel	Frozen	Active	Triplet	Singlet	Ground-state neutral	Triplet dication	Singlet dication
$C_2H_4^{2+}$	all	2	8	23×10^6	41×10^6	1	4	0
$C_2H_2^{2+}$	C-C stretch	2	8	9×10^6	14×10^6	8	8×1	8×1
$C_2H_2^{2+}$	C-H stretch	2	9	18×10^6	31×10^6	8	3×1	5×1

electrons determines the final states of the dication that are populated (e.g. [31], for PDI of Ar). The quantum numbers of the escaping electron pair that determines the symmetry are the orbital angular momentum L, spin S, and parity Π. When these quantum numbers are all odd or all even, the two-electron wave function has no nodes at the Wannier point, which is the optimal configuration of both electrons to be emitted into the continuum (they are equidistant from the ion with equal radial velocity at 180° to each other); the resulting dicationic state is then favorable. The cross section of such a reaction is then proportional to E^n, where E is the excess energy above threshold and $n > 1$ (as introduced by Wannier [32]) or a modulated linear function of E [33]. These symmetry requirements, when applied to the PDI of centrosymmetric closed shell molecules, translate into a propensity rule that favors mainly the singlet ungerade and triplet gerade states of the dications to be populated [5,30]. While going from a spherical symmetric atom to a centrosymmetric closed-shell molecule the reduction in symmetry removes all effect from the orbital angular momentum restriction. The selection rule would further weaken for the open-shell case when even S and Π lose their restrictive influence. It is worth pointing out that, while our measurements with photon energies about 10 eV above the first double-ionization threshold of ethylene and acetylene molecules are noticeably higher than the original Wannier region, there are previous PDI studies on atoms and molecules (for example [34–36],) that show that the Wannier region can be extended to many tens of eV above the threshold (similar to or even higher than the photon energies used in the present studies) and verify that the selection and propensity rules based on Wannier's theory can still be applied.

In a scenario different from that discussed in the preceding paragraph, for example, the core electron ionization, followed by Auger decay, favors the population of singlet states (both gerade and ungerade symmetry) as opposed to triplet states [10,37,38]. The contribution of triplet states from closed-shell molecules in the Auger decay to the PDI is low [10,37,38] due to a small overlap integral. The Auger decay probability, based on the simplest spin-restricted theory, depends on a two-electron Coulomb integral involving a core orbital, a continuum orbital, and two valence orbitals. For triplet states the orbitals of the two valence electrons involved in the process must be different. Hence the transition matrix element involves the antisymmetric combination of two spatial integrals that tend to cancel for high-energy continuum orbitals [37]. For simplicity, we refer to the former as the propensity rule (valence) and the latter as the propensity rule (Auger) for the rest of this paper.

III. CALCULATIONS

We have performed calculations of the potential-energy surfaces of excited dications using the Columbus quantum chemistry program [39–43]. We calculate one-dimensional cuts that pass through the equilibrium geometry of the ground-state neutral ethylene, which is taken to be $R_{CC} = 2.5303$ bohrs, $R_{CH} = 2.0522$ bohrs, and $\theta_{HCH} = 117.6°$, the same as in Ref. [6]. We have used $R_{CC} = 2.2871$ bohrs and $R_{CH} = 2.0103$ bohrs for acetylene. Excited-state energies were calculated using configuration-interaction with single and double excitations with Dunning's aug-cc-pvtz basis set [44]. The reference spaces included the 10 valence orbitals of acetylene and ethylene, with 11 orbitals used for the acetylene C-H stretch calculation, including an additional a' orbital in c_S symmetry. The $1s$ orbitals were frozen and therefore the reference spaces were 10 electrons in 8 orbitals, 12 in 8, and 12 in 9 for the ethylene, acetylene C-C stretch, and acetylene C-H stretch calculations, yielding 41×10^6, 14×10^6, and 31×10^6 configurations for singlets and 23×10^6, 9×10^6, and 18×10^6 for triplets, respectively. The orbitals were obtained by state-averaged multiconfiguration self-consistent-field calculations in which weighted averages of neutral and dication states' energies were minimized. For the ethylene calculations the ground neutral and $^3A_u(T_1)$ dication state energies were averaged with a weight of 1:4. For the ten-orbital acetylene C-C stretch calculations, the ground state with weight 8 and the first eight singlet and triplet dication states with weights one were averaged; for the 11-orbital C-H stretch calculation, the ground state with weight 8 and the first five singlets and three triplets with weights one were averaged. All these parameters are also summarized in Table I. Previous calculations of the excited states of ethylene can be found in Refs. [6–8,45–48] and those of acetylene in Refs. [11,14,16,49,50].

The configuration-interaction method is in general not size consistent and is expected to overestimate the dissociation energies. The dissociation under study include the fragments with no (H^+) or one (H_2^+) electron. For those fragments, the size consistency issue inherent in the configuration interaction does not apply. Calculated kinetic-energy releases are given without any adjustment. Those for the C-C dissociation should in general be expected to be too low.

IV. RESULTS AND DISCUSSION

We have measured the PDI of ethylene and acetylene using linearly polarized light of 40.5- and 42-eV photon energy, respectively.

TABLE II. Vertical DIPs for the electronic states of the ethylene dication at the geometry $R_{CC} = 2.5303$ bohrs, $R_{CH} = 2.0522$ bohrs, and $\theta_{HCH} = 117.6°$. The column labeled "Prop." denotes whether or not the state is preferred by the propensity rule (double-ionization preferentially populates singlet ungerade and triplet gerade states). The channel label denotes the dication breakup channels as (I) $H^+ + C_2H_3^+$, (II) $CH_2^+ + CH_2^+$, and (III) $H_2^+ + C_2H_2^+$, respectively. The state is check marked if it appears to be able to dissociate directly or labeled with the intersecting state if there is a likely dissociative pathway via a single conical intersection. The label B denotes that there is a barrier in the dissociative degree of freedom, however, the dissociation may still happen by over the barrier.

		Channels			Vertical DIPs		
State	Prop.	I	II	III	Present	Calc [6].	Expt.
^1A_g (S_1)			B		30.20	29.46	
^3A_u (T_1)		B			31.17	30.65	31.4 [48]
^1A_u (S_2)	✓	B	S_1		31.76	31.19	30.9 [18]
$^3B_{3u}$			✓		33.71	32.78	
^1A_g (S_3)		✓	S_1,$^1B_{3u}$		34.18	33.93	34.3 [18]
$^3B_{1g}$	✓		$^3B_{3u}$	✓	34.29	33.73	
$^1B_{3u}$	✓	S_3	✓		34.64	33.81	
$^1B_{1g}$			$^1B_{3u}$	✓	35.47	34.87	
$^3B_{3g}$	✓	B	$^3B_{3u}$		35.56	34.96	
$^3B_{1u}$			$^3B_{3u}$	✓	35.93	35.92	
$^1B_{3g}$		✓	$^1B_{3u}$		36.75	36.31	36.2 [18]
$^3B_{2g}$	✓		✓		37.59	36.87	
^1A_g (S_4)						38.37	

A. Ethylene (C_2H_4): $E_\gamma = 40.5$ eV

The following channels are observed in our measurements on the PDI of ethylene:

$$C_2H_4 + E_\gamma \rightarrow {C_2H_4}^{2+} + 2e^- \quad \text{NDI}$$

$$\left.\begin{aligned} &\rightarrow H^+ + C_2H_3^+ + 2e^- \quad \text{(deprotonation)} \\ &\rightarrow CH_2^+ + CH_2^+ + 2e^- \quad \text{(symmetric)} \\ &\rightarrow H_2^+ + C_2H_2^+ + 2e^- \quad \text{(asymmetric)} \end{aligned}\right\} \text{DI},$$

where E_γ represents the photon energy. Table II summarizes the results of the electronic-structure calculations and includes the calculated vertical ionization potentials from the equilibrium geometry of the parent molecule, a note as to whether or not the electronic state is preferred by the propensity rule (valence), and a note as to whether or not the electronic state is dissociative for each fragment channel either directly or via likely conical intersections.

We have used the typical COLTRIMS analysis of multiparticle coincidence and TOF measurements to isolate the DI channels in the data, as shown in Fig. 2(b). However, to isolate the NDI channel we exploit the available position measurement as well as the TOF, as shown in Fig. 2(a).

A useful tool for channel identification is the so-called photoion-photoion coincidence (PIPICO) spectrum, where the yield is plotted as a function of the TOF of the first and second recoil ions, as shown in Fig. 2(b). Two paired fragment ions resulting from a breakup channel form a stripe in the PIPICO spectrum (also, e.g. [27,51–54],). We have observed three different breakup channels: deprotonation ($H^+ + C_2H_3^+$), symmetric breakup ($CH_2^+ + CH_2^+$), and asymmetric breakup ($H_2^+ + C_2H_2^+$). By selecting the TOF of the ions and applying momentum conservation we can single out particular breakup channels and calculate the full three-dimensional momentum vector of the ions and their respective electrons. For the DI we use the E_{sum} of these electrons together with the KER of the fragment ions to determine the populated electronic state of the parent dication and the asymptotic final energy. Once determined, these values are used to trace the path the molecule took through the PES, as discussed in the following sections.

Branching ratios of the DI channels are obtained by considering two electrons measured in coincidence with two fragment ions. In the case of the NDI channel we look for the yield of both photoelectrons in coincidence with the metastable dication. The branching ratio for each of these channels is presented in Table III. In the cases of two overlapping peaks in the E_{sum} spectrum we fit two Gaussian distributions for each of these peaks such that the sum of the two fits matches the measured distribution. Note that we cannot measure absolute cross section using COLTRIMS but produce relative yields only.

The ionization yield must also be corrected for the detector efficiency, which depends on the number of coincident particles used to isolate an event. In the case of NDI two electrons and one recoil ion are recorded, but for the other DI channels two ions and two electrons must be recorded in coincidence. For the correction factor we have used the particle detection efficiency ($\epsilon_{particle} = 0.48 \pm 0.1$) given by the product of the open-area ratio of the microchannel plate detectors (about $60 \pm 10\%$) as a maximum detection efficiency and the transmission (about $80 \pm 10\%$) of the spectrometer grid in front of the ion detector.

1. NDI: $C_2H_4^{2+}$

The NDI channel results in a metastable molecular dication ($C_2H_4^{2+}$) and two photoelectrons. These dications can be separated and identified from other ions by their TOF, position on the detector, and in a more advanced analysis the energy of the two electrons. The TOF of the ions in the static field of the spectrometer is proportional to their mass to charge ratio, which distinguishes the $C_2H_4^{2+}$ channel from the single- and double-ionization channels as shown in Fig. 2(a). To distinguish the $C_2H_4^{2+}$ channel from the CH_2^+ channel (which shares the same mass to charge ratio), the position and the TOF spread must be examined. In contrast to the CH_2^+ channel, the metastable dications have a small kinetic energy and therefore are sharply peaked in both TOF and detector position.

A metastable dication requires a local potential well and a barrier to prevent immediate fragmentation. Note that the lifetime of the detected dications must be greater than their TOF (4.1 μs). In Ref. [8] the barrier to deprotonation on the ground singlet state of the dication (S_1 at the equilibrium geometry of the neutral) was calculated as 68.8 kcal/mol and for a symmetric breakup as 88.4 kcal/mol. Given the vertical transition energy of 30.2 eV calculated for the S_1 state, these barriers lie at 33.2 and 34 eV. We therefore would expect that the S_1 state supports long-lived vibrational states.

While plotting the kinetic energy of electron 2 as a function of the kinetic energy of electron 1 in Fig. 2(c) (note that the

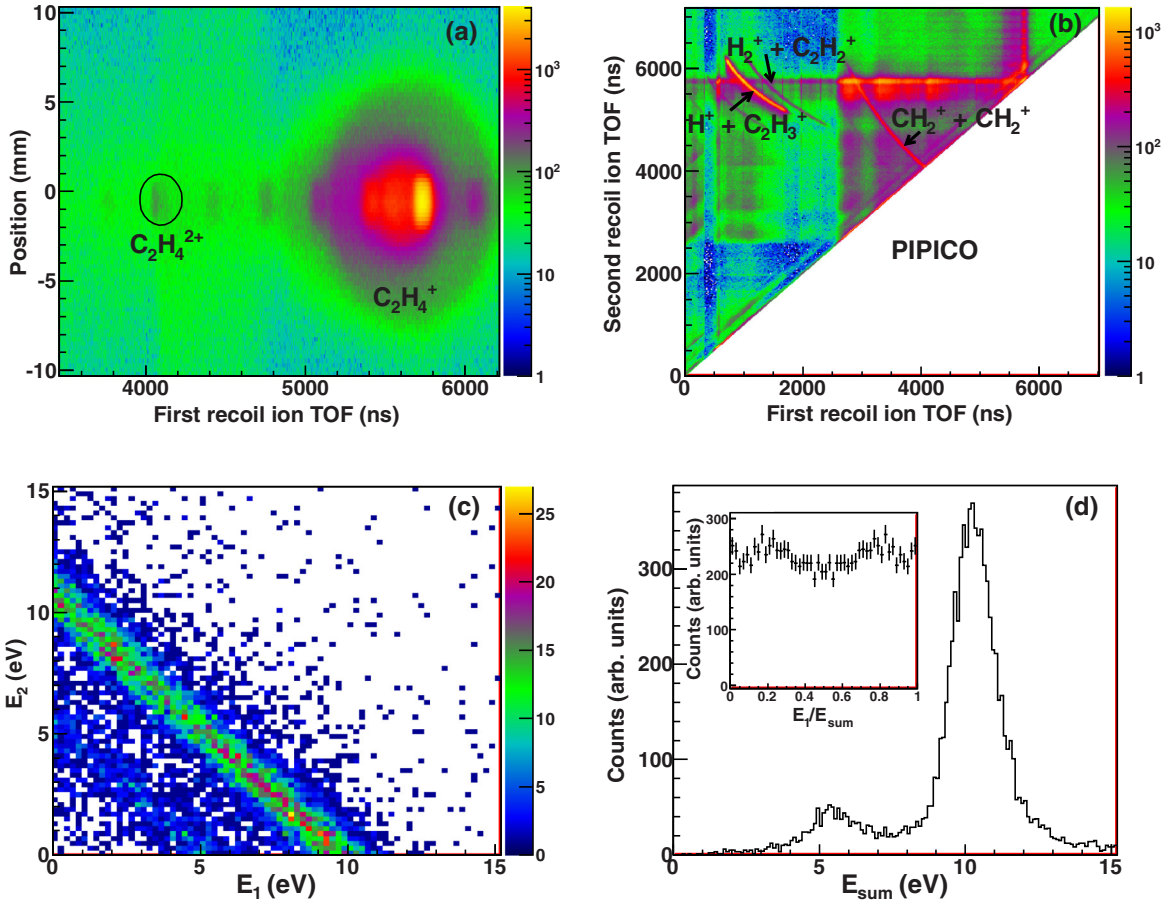

FIG. 2. (Color online) Separation of different channels in the direct photo-double-ionization of ethylene at 40.5-eV photon energy. (a) Density plot of the TOF of the recoil ions and their position on the detector to trace the metastable dication (nondissociative ionization). (b) Photoion-photoion coincidence spectrum for the separation and identification of different breakup channels in time (dissociative ionization). (c) Density plot of the kinetic energy of the two electrons measured in coincidence with the ethylene dications. (d) Electron sum kinetic energy $E_{\rm sum}$ of the two electrons described in (c). The inset in (d) is the plot of the ratio $E_1/E_{\rm sum}$ for the $E_{\rm sum}$ peak around 10.2 eV. For the error bars in this $E_{\rm sum}$ distribution refer to Fig. 4, where it is presented as threshold energy.

numbering of the particles is arbitrary) we find two diagonal lines obeying the energy conservation law. The energy-sharing distribution, plotted as the ratio of one electron kinetic energy to the sum kinetic energy of both electrons, for the main peak of the $E_{\rm sum}$ at 10.2 eV is shown in the inset of Fig. 2(d). The flatness is stemming from direct photo-double-ionization processes only. One may wonder if the residual structures in the data may be due to contributions of higher orders in the Coulomb-dipole theory [33], however, given our statistical error bars we do not believe that such an effect can be observed here. Previous measurements of the PDI of argon [31] could not observe such contributions either, although this target was less complex, had a higher atomic number Z, and a rather well-defined radius compared to the ethylene molecule, where any dipole interaction is less well determined and may exhibit interferences. No traces of secondary processes such as Auger decay or autoionization, which would show up as distinct islands in Fig. 2(c) and result in an asymmetric energy sharing, are visible. Similar plots for the DI channels (not shown here) help us to verify that at least 80% of the double-ionization events detected for both targets C_2H_4 and C_2H_2 so close to threshold originate from direct double ionization. The small percentage due to two-step processes will not be discussed in the present article. However, for the NDI two separate features can be clearly distinguished in Figs. 2(c) and 2(d). The main peak of the distribution in Fig. 2(d), at around 10.2 eV, indicates that the threshold of the double ionization is at about 30.3 eV, which is in agreement with the previously reported values [6,7,17]. The vertical energy for this feature ($E_{\rm sum} = 10.2$ eV) of the NDI is 30.3 eV. One can assume that these dications are produced in the lowest manifold of states, i.e., the electronic ground singlet state ^1A_g ($=S_1$), lowest triplet state ^3A_u ($=T_1$), or the electronic first excited singlet state ^1A_u ($=S_2$) of the ethylene dication. However, a survey of the double-ionization potentials (DIPs) presented in Table II shows that only S_1 has the right DIP (30.2 eV) in the Franck-Condon region. The T_1 and S_2 states have slightly higher DIPs, 31.17 and 31.76 eV, respectively. Therefore, the most likely candidate for the main feature is the S_1 state with a 30.2-eV DIP.

The S_1 state exhibits barriers [8] in the deprotonation (33.2-eV) and symmetric breakup (34-eV) channels and can therefore support the production of a metastable dication. However, the S_1 state is not favored by the propensity rule

TABLE III. Electron sum kinetic energy E_{sum}, vertical energy E_{vert}, KER, the states involved, and the branching ratio of different channels measured in the photo-double-ionization of C_2H_4 using 40.5-eV photons. All energies are in eV. We estimate the absolute photoionization cross sections for different breakup channels at 40.5-eV photon energy by referring to the absolute H_2^+ photoionization cross section of 0.07 Mb from Ref. [24] (assuming that the H_2^+ production there solely stems from the H_2^++$C_2H_2^+$ channel). The photoionization cross sections for $C_2H_4^{2+}$, $H^+ + C_2H_3^+$, and $CH_2^+ + CH_2^+$ channels are thus 0.05, 0.62, and 0.24 Mb, respectively.

Channels	E_{sum}	E_{vert}	KER	States	Branching ratio (%)
$C_2H_4^{2+}$	10.2	30.3		S_1	5.0 ± 0.8
	5.5	35		$^3B_{1g}$,$^3B_{1u}$	0.4 ± 0.1
$H^+ + C_2H_3^+$	6.5	34	4.3	S_3	29.5 ± 4.3
	8.7	31.8	4.3	S_2	25.8 ± 3.7
	9.5	31	3.8	T_1	8.1 ± 1.2
$CH_2^+ + CH_2^+$	5	35.5	5.5	$^1B_{3u}$,$^3B_{3g}$	22.6 ± 3.4
	7	33.5	4.1	$S_2 \Rightarrow S_1$	1.5 ± 0.2
$H_2^+ + C_2H_2^+$	5	35.5	4.4	$^{1,3}B_{1g}$,$^3B_{1u}$ $^{1,3}B_2$	7.1 ± 1.1

(valence) introduced above. From our measured branching ratio presented in Table III, this channel still contributes to about 5.0% to the direct PDI of ethylene near threshold. In this regard the propensity rule (valence) appears to be weak. Later on we test this assertion by using the K-shell ionization of ethylene followed by Auger decay. In Auger decay the propensity rule (valence) does not apply and the S_1 state is favored by the propensity rule (Auger) and hence is expected to be populated more (see Sec. IV A 6).

We also observe a minor peak at around 5.5 eV in Fig. 2(d). This feature has a very small branching ratio (about 0.4% of the total double-ionization yield) and results from dications that are formed in highly excited electronic states with a vertical energy of about 35 eV. Based on the vertical energy, the likely states are $^3B_{3u}$, $^1A_g(S_3)$, $^3B_{1g}$, $^1B_{3u}$, $^1B_{1g}$, $^3B_{3g}$, and $^3B_{1u}$. The $^3B_{3u}$ state has a DIP (33.71 eV) that is lower than the vertical energy. This state undergoes a large excursion in the C-C stretch and hence is an unlikely candidate, however, it is bound in the C-H coordinate. The S_3 state has a DIP (34.18 eV) that is lower than the vertical energy. This state is dissociative along the C-H coordinate and hence not a likely candidate for this feature. The states $^1B_{3u}$ (DIP of 34.64 eV) and $^1B_{1g}$ (DIP of 35.47 eV) are also unlikely as they couple to the S_3 and S_2 states via a large C-C stretch. We can also exclude $^3B_{3g}$ as it couples to $^3B_{3u}$ and $^3B_{1g}$ via a C-H stretch. The remaining states $^3B_{1g}$ and $^3B_{1u}$ are the most likely states. The state $^3B_{1g}$ (DIP of 34.29 eV) is bound in the C-H coordinate, has smaller excursion in the C-C stretch, and may couple to T_1, but it is favored by the propensity rule (valence). The other plausible state for this feature is $^3B_{1u}$, with a DIP (35.93 eV) slightly higher than the vertical energy, but it is not favored by the propensity rule (valence).

2. *Deprotonation:* $H^+ + C_2H_3^+$

We present the yield as a function of E_{sum} and KER for three different DI channels in Fig. 3. These spectra provide information on the correlation of the electrons and nuclear fragments in the breakup. The projections of these spectra along the horizontal and vertical axes give the KER and the E_{sum} distributions (not shown), respectively. The measured KER is an additional tool available in the DI channels to help identify the populated states. In order to identify the most likely electronic states involved, the states in the vicinity of the vertical energy (i.e., $E_\gamma - E_{sum}$) are singled out first. Then we check for barriers in the given coordinate and matching KER (for dissociative states) in addition to the validity of the propensity rule (valence). We have listed the likely states for different channels in Table III.

The KER for the deprotonation channel ($H^+ + C_2H_3^+$) is a narrow distribution, which peaks at around 4.3 eV, while the E_{sum} distribution is wider and exhibits two peaks [at about 6.5 and 8.7 eV marked with two ellipses in Fig. 3(a)]. We have identified these two peaks by looking at the experimental vertical energy given in Fig. 4 (open blue circles). The presence of the two peaks in the E_{sum} distribution indicates that at least two different manifolds of electronic states are populated in the ionization step. This leads to two different fragmentation pathways.

Let us first consider the deprotonation channel with an E_{sum} peak at 6.5 eV that gives a vertical energy of 34 eV. According to the DIP energy the possible states are ^1A_g (i.e., the S_3 state,

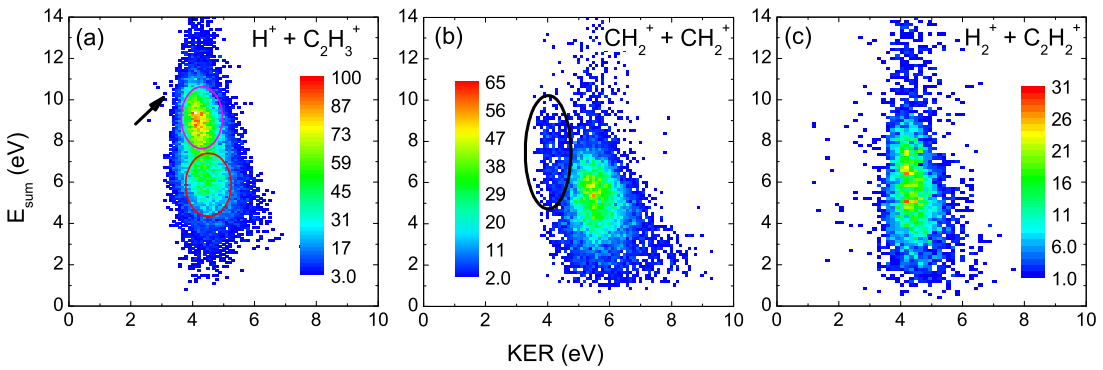

FIG. 3. (Color online) Energy correlation map between the ionic KER along the horizontal axis and the E_{sum} along the vertical axis for the (a) $H^+ + C_2H_3^+$, (b) $CH_2^+ + CH_2^+$, and (c) $H_2^+ + C_2H_2^+$ channels of ethylene using 40.5-eV photons. The color scale is linear and the dynamic range is about the same for all plots.

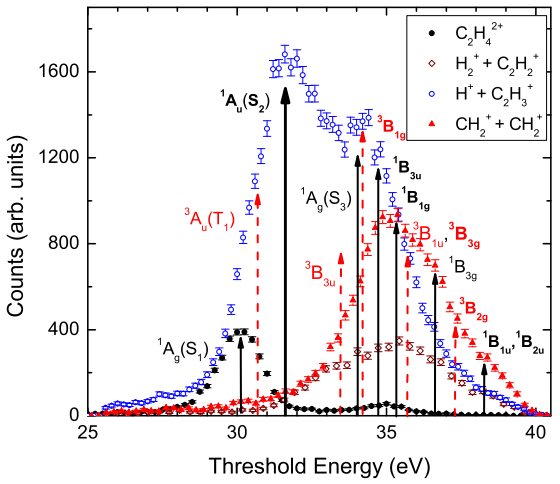

FIG. 4. (Color online) Ionization yield as a function of threshold energy, defined as $E_{\rm sum}$ subtracted from E_γ (40.5 eV, linearly polarized), for all PDI channels of ethylene. This energy is equivalent to the vertical energy on the potential-energy surface, which is crucial to identify the ionization pathways. The error bars represent the statistical errors only. The distribution is corrected for the higher detection efficiency of the NDI channel (black solid circles) compared to the ion-pair channels. The relevant states are indicated with vertical arrows (solid black lines for singlet and red dashed lines for triplets) based on their DIPs. States in bold are favored by the propensity rule (valence).

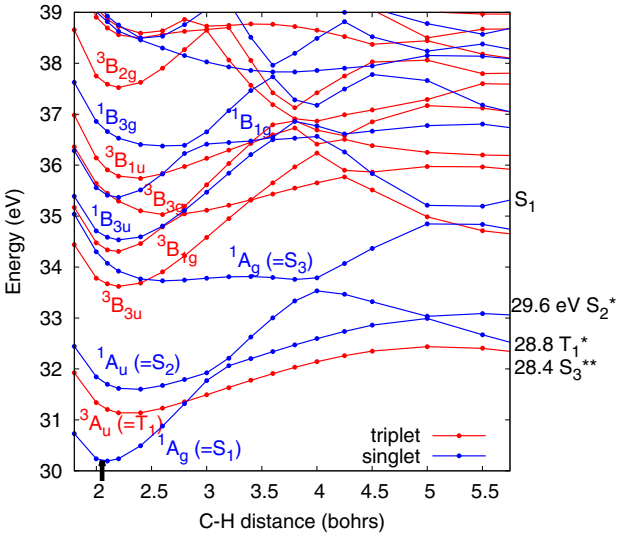

FIG. 5. (Color online) Cut of the PESs (singlet and triplet states) of the ethylene dication for C-H distance calculated using the multiconfiguration self-consistent field method. The Franck-Condon region is indicated with an arrow at the bottom on the horizontal axis. The energies of the asymptotes of the diabatic S_2, S_3, and T_1 states within this cut are given on the right side. The double asterisk indicates that the asymptote of the diabatic S_3 state is approximately 1.5 eV lower in the linear CH_2-C-H geometry compared to the planar geometry. A single asterisk indicates that the asymptotes of the S_2 and T_1 are 1 eV higher at such (planar) geometries than in the linear CH_2-C-H geometry. States are labeled with the d_{2h} irreducible representations appropriate at the equilibrium geometry of the neutral.

with a DIP of 34.18 eV), $^3B_{1g}$ (DIP of 34.29 eV), and $^1B_{3u}$ (DIP of 34.64 eV). These states are shown in Fig. 5 as a function of the C-H distance. The energy difference between the vertical energy and the DIP can point to a vibrational excitation of the dications in a particular state. Vibrational excitations can lead to a broad $E_{\rm sum}$ distribution for a given KER. In Fig. 3(a) one can see that the KER distribution is relatively narrow compared to the $E_{\rm sum}$ distribution, indicating the influence of vibrational excitation in our measurements. Note that in the DI channels the fragments (with the exception of free protons) can be vibrationally excited.

A vertical DIP of 34.18 eV is given by our configuration-interaction calculations for the $^1A_g(S_3)$ state shown in Fig. 5. This state is not clearly bound in the C-H stretch direction and is therefore the only candidate for the 6.5-eV deprotonation peak. The experimental vertical energy may be compared with a recent calculation of 33.94 eV [6] and previous values ranging from 33 to 36 eV. In the cut in Fig. 5 the H-C-C angles are all held constant at 121.2°. The linear (CH_2)-C-H geometry corresponds to a local minimum on the $C_2H_3^+$ cation ground-state singlet potential-energy surface, which is approximately 1.5 eV lower than depicted. The asymptotes of the diabatic S_2 and T_1 states in Fig. 5 are, in contrast, approximately 1 eV higher in the linear (CH_2)-C-H geometry compared to the geometry where the H-C-C angles are all held constant at 121.2°.

The one-dimensional cut in the potential-energy surface of the $^1A_g(S_3)$ state, shown in Fig. 5, is flat when approaching the avoided crossing with the $^1A_g(S_1)$ state at approximately 4 bohrs. Furthermore, as shown in Fig. 6, the S_3 state is metastable with respect to the C-C stretch (although the conical intersection with the S_1 state will allow some C-C dissociation

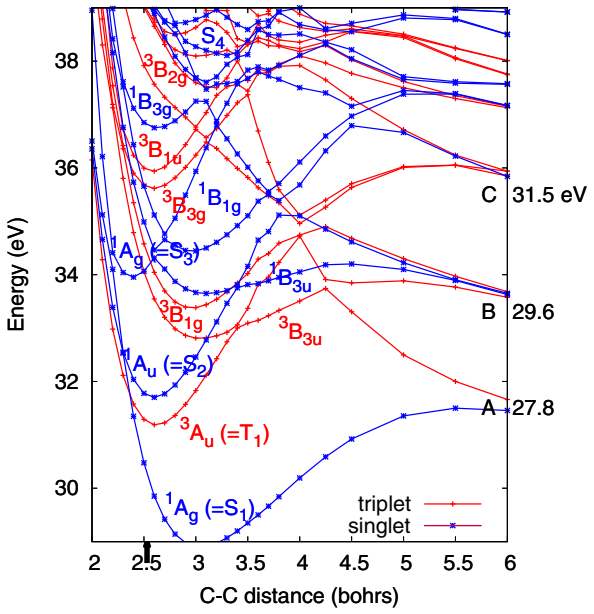

FIG. 6. (Color online) Cut of the PESs (singlet and triplet states) of the ethylene dication as a function of the C-C distance calculated using the multiconfiguration self-consistent field method. The arrow at the bottom indicates the Franck-Condon region. The asymptotes A, B, and C correlate with the A' and A'' components of the ground $^2\Pi$ state of both CH_2^+ fragments. With CH_2^+ being linear these asymptotes are degenerate at approximately 27.8 eV.

via the S_1 state). The minimum-energy path to the avoided crossing must be lower in energy than the path depicted in Fig. 5 and therefore the avoided crossing will be accessible by a downhill path from the initial geometry. Furthermore, it is likely that an accidental conical intersection [55] between these two states exists and is accessible, though we have found no discussion of this point in the literature.

The diabatic S_3 state correlates with the ground state of the $C_2H_3^+$ cation. The state then proceeds to a conical intersection with the $^1A_u(S_2)$ state at approximately 5 bohrs in Fig. 5. The diabatic S_3 state continues to become the lowest asymptote. The diagram implies two options for the dissociative mechanism: dissociation on the diabatic S_2 asymptote with a peak KER of 4.6 eV and dissociation on the diabatic S_3 state with maximum and peak KER values of 7.3 and 5.8 eV, respectively. The narrow distribution of the measured KER supports the former mechanism, but the multidimensional nature of the landscape on which the dynamics occurs precludes a conclusion on this point. It should be noted that an adiabatic transition to the diabatic S_2 asymptote (an avoidance of the conical intersection) occurs for nonplanar dication geometries only, i.e., a molecular conformation change is indispensable since the neutral molecule's ground state is planar.

In a similar way, we have identified two more states (S_2 and T_1; see Table III) contributing to another feature in the deprotonation (i.e., E_{sum} peak around 8.7 eV). This feature corresponds to a vertical energy of 31.8 eV. The S_2 state, favored by the propensity rule (valence), has a DIP of 31.76 eV. The lowest triplet T_1 state has a DIP of 31.17 eV but is not favored by the propensity rule (valence) and contributes to the shoulderlike feature only (discussed below). The S_2 and T_1 states have similar behaviors in the C-H and C-C stretch, as can be seen in Figs. 5 and 6. The superior agreement of the calculated DIP of the S_2 state with the observed DIP (31.8 eV), along with its satisfaction of the propensity rule (valence), supports the assignment of the E_{sum} peak at the 8.7-eV feature to this state.

Once S_2 is populated there are a number of possible pathways to dissociation. Without enumerating the many options, note that if the dissociation proceeds to the diabatic S_3 asymptote via a conical intersection between the S_2 and diabatic S_3 states, the maximum KER is approximately 4.9 eV. This is very close to the value we have measured. We conclude that this pathway is responsible for the deprotonation channel with a vertical energy of 31.8 eV.

A careful inspection of the threshold energy spectrum of the deprotonation channel, displayed in Fig. 4 (open blue circles), reveals a shoulderlike structure just above 30 eV. This is a result of the dication population in the T_1 state dissociating along the C-H bond. For this process to occur, the initial ionization step must populate the T_1 state with sufficient energy (e.g., by vibrational excitation) to surmount the potential barrier to dissociation. The top of the barrier is near 32.4 eV (see Fig. 5) and the dissociation leads to a KER value of 3.6 eV. The feature is visible in Fig. 3(a) as counts below 4-eV KER and is marked with an arrow based on the E_{sum} and KER values.

3. Symmetric breakup: $CH_2^+ + CH_2^+$

The symmetric breakup channel data, shown in Fig. 3(b), is comprised of two features: a dominant peak with E_{sum} and KER centered at about 5 and 5.5 eV, respectively, and a minor shoulderlike feature with a broad E_{sum} distribution around 7 eV with a narrow KER peak at 4.1 eV. We begin the discussion with the major feature. The vertical energy of 35.5 eV suggests the following states as possible candidates: $^{1,3}B_{3u}$, $^1A_g(S_3)$, $^{1,3}B_{1g}$, $^{1,3}B_{3g}$, and $^3B_{1u}$; all are shown in Fig. 6 as a function of the C-C distance.

The $^3B_{3u}$ (DIP of 33.71 eV) and S_3 (DIP of 34.18 eV) are too low in their vertical energy, not favored by the propensity rule (valence), and hence are not likely candidates. As mentioned in the previous section, S_3 dissociates by deprotonation. Given that the reduced mass in the C-H degree of freedom is small, the deprotonation will strongly compete with the symmetric breakup on the S_3 state. The $^3B_{1g}$ (DIP of 34.29 eV) state is favored by the propensity rule (valence), but its vertical DIP appears to be too low in comparison to the experimental value. It is also an unlikely candidate due to its inability to couple to $^3B_{3u}$. The other states, namely, $^1B_{1g}$ (DIP of 35.47 eV), $^3B_{1u}$ (DIP of 35.93 eV), and $^1B_{3g}$ (DIP of 36.75 eV), are not favored by the propensity rule (valence).

The $^1B_{3u}$ (DIP of 34.64 eV) and $^3B_{3g}$ (DIP of 35.56 eV) states are favored by the propensity rule (valence) and considered the most likely candidates. The $^1B_{3u}$ state is dissociative along the C-C coordinate and the expected KER is 5 eV. The $^3B_{3g}$ state is bound along the C-C coordinate near the Franck-Condon region, but it intersects directly with the dissociative $^3B_{3u}$ state. The expected KER of this path is 5.96 eV. Both KER values agree with our measured KER peak value of 5.5 eV.

The shoulderlike feature in the KER distribution at around 4.1 eV [marked with an ellipse in the density plot in Fig. 3(b)] amounts to about 1.5% of the total double-ionization yield. The pathway leading to this minor channel involves the S_1 and S_2 electronic states. A dissociation of the ethylene dication on S_1 leads to the breaking of the central C-C bond, which then produces two CH_2^+ ions [6]. We suggest that the fragmentation pathway to this minor channel starts with the population of the S_2 state, which is allowed by the propensity rule (valence). This population transfers to the S_1 state of the dication via the conical intersection. Any extra energy can go into electronic or vibrational excitations of the product ions (both are molecular ions in this symmetric breakup channel). The expected KER for the fragmentation of the dication in the electronic ground state is 4.0 eV and is close to our measured KER of 4.1 eV.

4. Asymmetric breakup: $H_2^+ + C_2H_2^+$

The $H_2^+ + C_2H_2^+$ channel energy map in Fig. 3(c) has a KER distribution peak around 4.4 eV and a broad E_{sum} distribution peaking around 5 eV (corresponding to a vertical energy of 35.5 eV) that is similar to the E_{sum} distribution of the symmetric channel. The hydrogen molecular ion (H_2^+) can be formed in the fragmentation of ethylene dication in two ways: (i) one of the hydrogen atoms travels across the C=C double bond forming an ethylidenelike (CH_3CH^{2+}) intermediate state [18,47], which is followed by a fragmentation that leaves an acetylene-type ion ($HCCH^+$) behind, and (ii) two hydrogen atoms that are initially bound to the same carbon atom form a bond between them and increase the distance to the parent ion, which results in a vinylidenelike (CCH_2^+) structure in

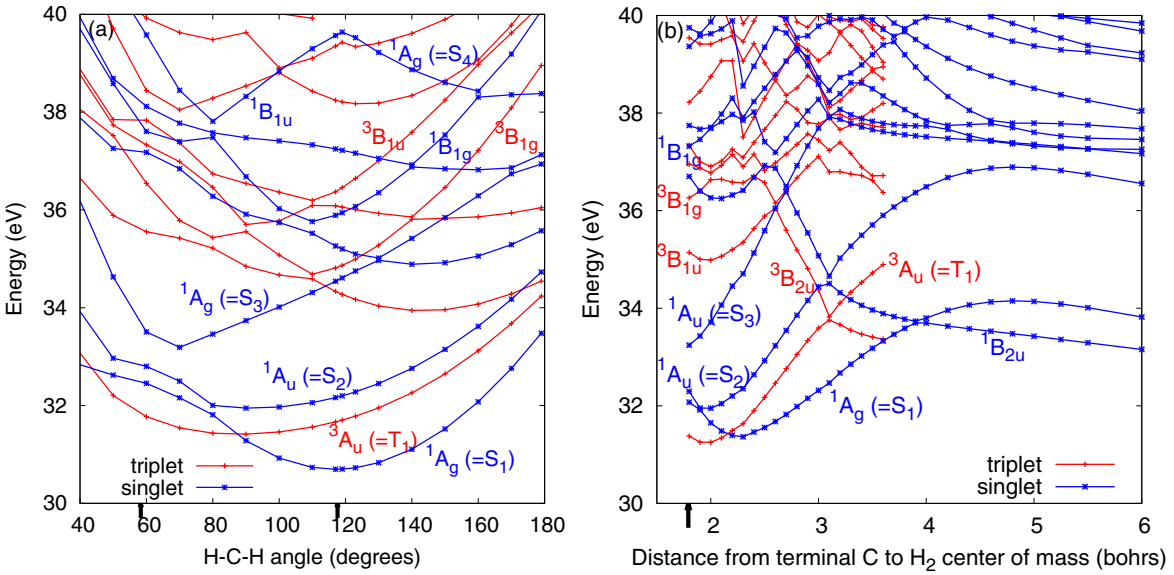

FIG. 7. (Color online) Cut of the PESs of the ethylene dication relevant to the asymmetric breakup ($H_2^+ + C_2H_2^+$) channel. (a) Potentials as a function of the H-C-H bending angle. The initial angle (117.6°) and the angle (58.3°) at which the H_2 distance is 2.0 bohrs are marked with arrows. (b) Potentials as a function of the distance between the last C (in C_2H_2 in the HHCC configuration) and the center of mass of H_2. The arrow corresponds to the arrow in (a) at 58.3°. States are labeled with the d_{2h} irreducible representations appropriate at the equilibrium geometry of the neutral.

the dissociation. Most likely both cases contribute to the yield of the asymmetric channel in our measurements. In order to identify the relevant states we consider only the latter direct asymmetric mechanism in our calculations and discussion.

With the given broad $E_{\rm sum}$ of 3 eV (full width at half maximum) no repulsive state in the C-H_2 coordinate can be populated directly. The pertinent states in the Franck-Condon region depicted in Fig. 7(b) exhibit barriers towards dissociation. We conclude that the H-C-H angle has to decrease first in order to circumnavigate these barriers on the PES. We therefore present the cut of the PESs as a function of the H-C-H angle in Fig. 7(a). The broad $E_{\rm sum}$ distribution indicates that several electronic states of the dication contribute to this dissociation channel. We consider electronic states that have a bonding H-H interaction, with potential-energy surfaces that comprise minima at small H-C-H bond angles. As proposed above, the distance between the terminal carbon atom and the center of mass of the two hydrogen atoms must now increase while the H-C-H bond angle decreases in order to circumnavigate the barriers in the C-H_2 coordinate and expel an H_2^+ fragment in the subsequent dissociation.

In Fig. 7(a) one can identify a number of singlet and triplet states with decreasing energy as the H-C-H angle decreases from its equilibrium value marked by the arrow at 117.6°. These are the $^{1,3}A_u$ (S_2 and T_1), $^1A_g(S_3)$, $^{1,3}B_{1g}$, and $^{1,3}B_{1u}$. The $^{1,3}B_{1g}$ and $^{1,3}B_{1u}$ states are likely populated based on their vertical energy at the equilibrium geometry. However, at the initial scissoring angle of 117.6° these states exhibit barriers towards dissociation in the C-H_2 coordinate [not shown in Fig. 7(b)] and hence do not dissociate immediately. In contrast, while undergoing a full scissoring mode reaching an H-C-H angle of 58.9°, the H-H bond distance would decrease to that of H_2^+ at its equilibrium geometry (i.e., 2.0 bohrs). This H-C-H angle is marked with an arrow in Fig. 7(a) and corresponds to the same geometry as that indicated by the arrow in the Fig. 7(b). While this H-H bond length may be considered favorable for expelling a stable H_2^+ ion, we can see that at a C-H_2 distance of 1.8 bohrs the dication states have potential barriers. Obviously, by the time the protons reached the equilibrium geometry of the H_2^+ ion the waging mode of the C-H_2 distance has progressed to a contracted ethylene dication. A hydrogen elimination must have taken place before this happens. We deduce that while the H-C-H angle was decreasing from the initial value of 117.6° during the approach of the potential minima, the C-H_2 distance was stretched beyond 2.6 bohrs from its value (around 1.0 bohr) at equilibrium. The C-H_2 distance of 2.6 bohrs is critical in order to couple to some low-lying repulsive states $^{1,3}B_{2u}$ via conical intersections.

In Fig. 7(b) one can see that these repulsive curves $^{1,3}B_{2u}$ are singlet and triplet states that correlate with the ground state of the vinylidene cation, which has A_1 symmetry in the c_{2V} point group and electronic configuration $1\text{-}4a_1^2 5a_1^1 1b_2^2 1b_1^2$; we have an additional singly occupied a_1 orbital, the $H_2^+\sigma_g$. We find that this configuration correlates with the transition $1b_{3g}^{-2}3a_g^{-1}3b_{1u}^{+1}$ from the ground-state neutral configuration, which gives the dication configuration $1\text{-}2a_g^2 3a_g^1 1\text{-}2b_{1u}^2 1b_{2u}^2 1b_{3u}^2 3b_{1u}^1$ overall $^{1,3}B_{2u}$ symmetry. Both repulsive dication states $^{1,3}B_{2u}$ have the same geometry and thus have the similar C-H_2 distance (around 3 bohrs) at the conical intersection, however, they differ in their energies by about 0.75 eV due to the different electron spin orientation. The $^{1,3}B_{2u}$ triplet and singlet states have about the same asymptotic limit in this geometry [not shown in Fig. 7(b)], which agrees with the much narrower KER spread than the $E_{\rm sum}$ distribution for this asymmetric channel. In conclusion, it seems plausible that the observed asymmetric dissociation is produced by a transition from the $^{1,3}B_{1g}$ and $^{1,3}B_{1u}$ states (populated by the

ionization step) through conical intersection to the $^{1,3}B_{2u}$ states that dissociate to the observed products.

5. Summary: Ethylene photo-double-ionization

The sum of the photo-double-ionization cross sections for the channels measured in this work is about 10% of the total photoabsorption cross section of 10 Mb at 40-eV photon energy [24,56,57]. We do not have a direct comparison for the double-ionization cross sections of ethylene estimated in this work to previous works, but a similar percentage of double ionization relative to the single ionization was observed for alkanes with two carbon atoms in Ref. [58].

We have found that, in the PDI of ethylene, the higher manifolds of the electronic excited states are responsible for all the DI channels as well as the minor feature in the NDI channel. The first excited electronic singlet S_2 state is directly responsible for the H^++$C_2H_3{}^+$ channel. In addition, the S_2 state creates the minor feature in the $CH_2{}^+$+$CH_2{}^+$ breakup via the conical intersection to the electronic ground state S_1.

There are a number of reasons to expect a higher branching ratio of metastable dications presented in Table III. First, there are multiple states with barriers in both C-H and C-C coordinates. Second, as discussed above, the T_1 and S_2 states of the ethylene dication, shown in Fig. 6, seem to have potential wells that may support a number of long-lived vibrational levels. Third, both Palaudoux *et al.* [59] and Furuhashi *et al.* [15] have reported vibrational levels in similar dication states of acetylene, though the potential wells in the acetylene dication are about 1 eV deeper than in the ethylene dication.

A high barrier to torsion of the molecular geometry on the S_1 state may explain the observed low NDI yield. Here we define the torsion angle as the angle between the planes containing the CH_2 group. The neutral molecule has a planar geometry with a torsion angle of 0° while the metastable electronic ground state of the dication has a twisted nonplanar geometry with a torsion angle of 90°. The change in geometry leads to small Franck-Condon factors as mentioned in Ref. [18].

The low NDI yield may also be caused by the propensity rule (valence), postulated 25 years ago [5,30,31]. The rule states that whenever two electrons are removed from a centrosymmetric closed-shell molecule in a direct double ionization by a single photon, predominantly the triplet gerade and singlet ungerade states of the dication are populated. In neutral ethylene the electronic ground state ^1A_g has the configuration $1a_g^2 1b_{1u}^2 2a_g^2 2b_{1u}^2 1b_{2u}^2 3a_g^2 1b_{3g}^2 1b_{3u}^2$ [6] (in D_{2h} symmetry group). The removal of two electrons from the outermost orbital $1b_{3u}^2$ results in the electronic ground state S_1 of the dication. This is a singlet state with A_g symmetry and hence is not favored by the propensity rule (valence). However, the $E_{\rm sum}$ value indicates that the majority of the NDI channel yields results from the S_1 state.

In spite of the small Franck-Condon factors and the propensity rule (valence) to produce a metastable dication in the PDI of C_2H_4, we have experimental evidence of the NDI channel (5.4%). The specific geometries of the electronic ground state of the neutral ethylene (planar) and the dication (nonplanar) lead to definitive Franck-Condon factors regardless of the ionization mechanism. However, the propensity rules are based on the ionization mechanism. We thus can test the applicability of the propensity rule (valence) by comparing the NDI channel yield in the Auger decay after core shell ionization (i.e., photoionization of a K-shell electron) to that of the PDI (i.e., removing two valence electrons in the ionization) of C_2H_4.

6. Comparison to Auger decay: C_2H_4

Dications of ethylene molecules can also be produced by single-photon ionization through Auger decay after K-shell ionization of the carbon atoms. This is an alternative mechanism useful in testing the effects of propensity rules in regard to the NDI channel.

We have measured this process by collecting the Auger electrons in coincidence with the recoiling ions after ionization by 310-eV photons (circularly polarized). In this measurement, the collection angle of the Auger electrons is limited to a cone of 12° with respect to the spectrometer axis. We implemented a retarding static electric field of about 20 V/cm to resolve the energy of the fast Auger electrons. The ion spectrometer arm retained a full collection angle of 4π for fragments from the ion-pair channels.

The main results from the Auger decay after K-shell ionization are summarized in Table IV. Surprisingly, we have detected a 5.3% metastable dication ($C_2H_4{}^{2+}$) branching ratio in both the K-shell ionization and PDI measurements while the branching ratios of the DI channels are very different. In terms of absolute cross sections, the NDI of the K-shell ionization (0.1 Mb) is also very similar to that of the valence ionization (0.05 Mb) within the uncertainty of our cross-section estimation (±50%). These cross sections are deduced from the data in the literature and our experimental branching ratios that are given in the captions of Tables III and IV. The yields of both the deprotonation and the asymmetric breakup channels have decreased and that of the symmetric channel has almost doubled in the K-shell ionization. The vertical energies for some DI channels in the Auger decay, shown in Fig. 8, are

TABLE IV. Auger electron kinetic energy $E_{\rm Auger}$, vertical energy $E_{\rm vert}$, KER, the states involved, and the branching ratio of different channels produced in the ionization of C_2H_4 by 310-eV photons. All energies are in eV. The photoabsorption cross section for ethylene at a photon energy of 310 eV is about 2 Mb [60]. Since the photon energy is above the carbon K-shell ionization threshold, we assume that the single ionization is followed by 100% effective Auger decay leading to the double ionization with the same absolute probability. The branching ratios given above for $C_2H_4{}^{2+}$, $H^+ + C_2H_3{}^+$, $CH_2{}^+ + CH_2{}^+$, and $H_2{}^+ + C_2H_2{}^+$ then translate to absolute cross sections of 0.11, 1.0, 0.87, and 0.02 Mb, respectively.

Channels	$E_{\rm Auger}$	$E_{\rm vert}$	KER	States	Branching ratio (%)
$C_2H_4{}^{2+}$	260	30.8		S_1	5.3 ± 1.0
$H^+ + C_2H_3{}^+$	257.5	33.3	4.5	S_3,S_2	46.3 ± 7.2
	265	25.8	4.5	satellite S_0 resonant Auger $[C(1s) \rightarrow \pi^*]$	3.6 ± 0.6
$CH_2{}^+ + CH_2{}^+$	254	36.8	5.9	$^1B_{3g}$,$^1B_{3u}$,S_4	41.1 ± 6.3
	258	32.8	4	$S_2 \Rightarrow S_1$	2.4 ± 0.4
$H_2{}^+ + C_2H_2{}^+$	253	37.8	4.6	$^1B_{1g,u}$,S_4,$^1B_{2u}$	1.2 ± 0.2

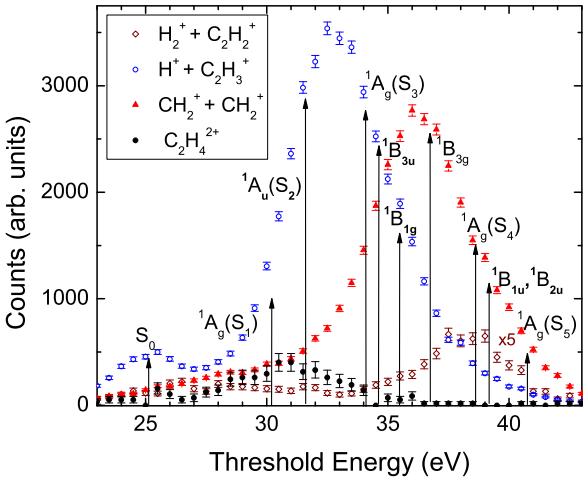

FIG. 8. (Color online) Same as Fig. 4 but for the K-shell ionization of ethylene by 310-eV photons (circularly polarized light).

also different from the PDI measurement at 40.5 eV. These differences may be caused by the propensity rule (Auger), which favors the population of singlet states (both gerade and ungerade symmetry) as opposed to triplet states in the Auger decay [37,38]. For this reason we have only listed the singlet states in Table IV and Fig. 8 as probable candidates. We have also observed an increased contribution from higher excited states in the DI channels produced by the Auger decay.

The Auger electron energy for the NDI ($C_2H_4^{2+}$) channel is 260 eV. With the carbon 1s ionization potential of 290.8 eV [61], the vertical energy is thus 30.8 eV. This vertical energy suggests that the dications are produced in the electronic ground state S_1 with a possible vibrational excitation. In contrast to PDI, the propensity rule (Auger) allows the S_1 state to be populated in the Auger decay. The surprising fact that there is almost no change on the NDI branching ratio between the two measurements, involving Auger decay and PDI, indicates that the propensity rules have little impact in the NDI channel. We conclude that the torsional barrier plays a larger role than the propensity rule (valance) in controlling the population of metastable dications of ethylene in the S_1 state.

For completeness we also briefly report on the DI channels produced by Auger decay and compare them to the PDI of C_2H_4. The deprotonation channel has an Auger electron energy of about 257.5 eV and a vertical energy of 33.3 eV. Compared to the multiple features observed in the PDI (see Fig. 4), we found one dominant channel in the Auger decay only, but the vertical energy is different (Fig. 8). The 33.3-eV vertical energy indicates that the S_3 state is populated and dissociates along S_2 through an avoided crossing. The expected KER of 4.6 eV is in agreement with the measured KER of 4.5 eV.

A minor contribution at an electron energy of about 265 eV (i.e., $E_{\text{vert}} = 25.8$ eV) is observed in the Auger decay (see Fig. 8). We can think of two processes responsible for this feature: (a) a satellite state resulting from the lowest unoccupied molecular orbital, i.e., it stems from the promotion of a π electron to an unoccupied π^* orbital [62,63], and (b) a resonant Auger decay following the $1s \rightarrow \pi^*$ excitation with ionization potential of about 285 eV [64]. Energetically both mechanisms are possible; however, given our experimental observable, we cannot separate their contributions at this photon energy. This feature is not observed in our PDI measurements.

The symmetric breakup retains features similar to those observed in the PDI data. The major feature (around $E_{\text{Auger}} =$ 254 eV) stems from electronic states with vertical energies around 36.8 eV. By surveying the PESs in Fig. 6, the likely states are $^1B_{3u}$ (DIP of 34.64 eV), $^1B_{3g}$ (DIP of 36.75 eV), and ^1A_g (S_4, DIP of 38.37 eV [6]). Though the DIP of the $^1B_{3u}$ state is low compared to that of the $^1B_{3g}$ state, the Auger electron energy distribution is broad enough to cover the energy range. The S_3 state may represent an alternative pathway, however, the estimated KER of 5 eV for this pathway is lower than the measured KER of 5.9 eV.

The pathway to the minor feature (around $E_{\text{Auger}} = 258$ eV) is similar to the one discussed in the PDI and involves the electronic states S_1 and S_2. A vibrationally excited population on the S_2 state feeds the S_1 state through a conical intersection and thereby dissociates along the C-C coordinate while breaking the central C=C bond.

The Auger electron energy for the asymmetric channel is 253 eV. As in the PDI, the singlet state $^1B_{1g}$ can be populated, which then dissociates via coupling to the $^1B_{2u}$ state. However, we notice only a small contribution of these states (see Fig. 8) at the corresponding Auger electron energy of 255 eV in the K-shell ionization. We instead observe Auger electrons at 253 and 251 eV. This suggests that the corresponding excited singlet states $^1B_{3g}$ and $^1A_g(S_4)$ are directly populated in the ionization process and dissociate via a coupling to the $^1B_{2u}$ state. In the PDI we also found triplet states that can couple to the repulsive $^3B_{2u}$ state via conical intersections and hence contribute to the yield of the asymmetric channel. However, since the population of triplet states is not favored by the propensity rule (Auger) in the K-shell ionization, the branching ratio of this asymmetric channel is smaller for the Auger decay compared to the PDI of valence electrons.

B. Acetylene (C_2H_2): $E_\gamma = 42$ eV

The following channels are observed in our measurements of the photo-double-ionization of acetylene using single linearly polarized 42-eV photons:

$$\begin{aligned} &C_2H_2 + E_\gamma \rightarrow C_2H_2^{2+} + 2e^- \qquad \text{NDI} \\ &\left.\begin{aligned} &\rightarrow H^+ + C_2H^+ + 2e^- \quad \text{(deprotonation)} \\ &\rightarrow CH^+ + CH^+ + 2e^- \quad \text{(symmetric)} \\ &\rightarrow C^+ + CH_2^+ + 2e^- \quad \text{(vinylidene)} \end{aligned}\right\} \text{DI.} \end{aligned}$$

These channels are identified and analyzed in a similar way as in the PDI of ethylene. The NDI of acetylene results in a metastable dication ($C_2H_2^{2+}$) and two free electrons. The energy correlation maps for the DI channels of acetylene are shown in Fig. 9. The measured E_{sum}, KER, and the vertical energies, the most likely electronic states, and the branching ratio of the different channels for the PDI of acetylene are presented in Table V. Table VI summarizes the results of the electronic-structure calculations on acetylene.

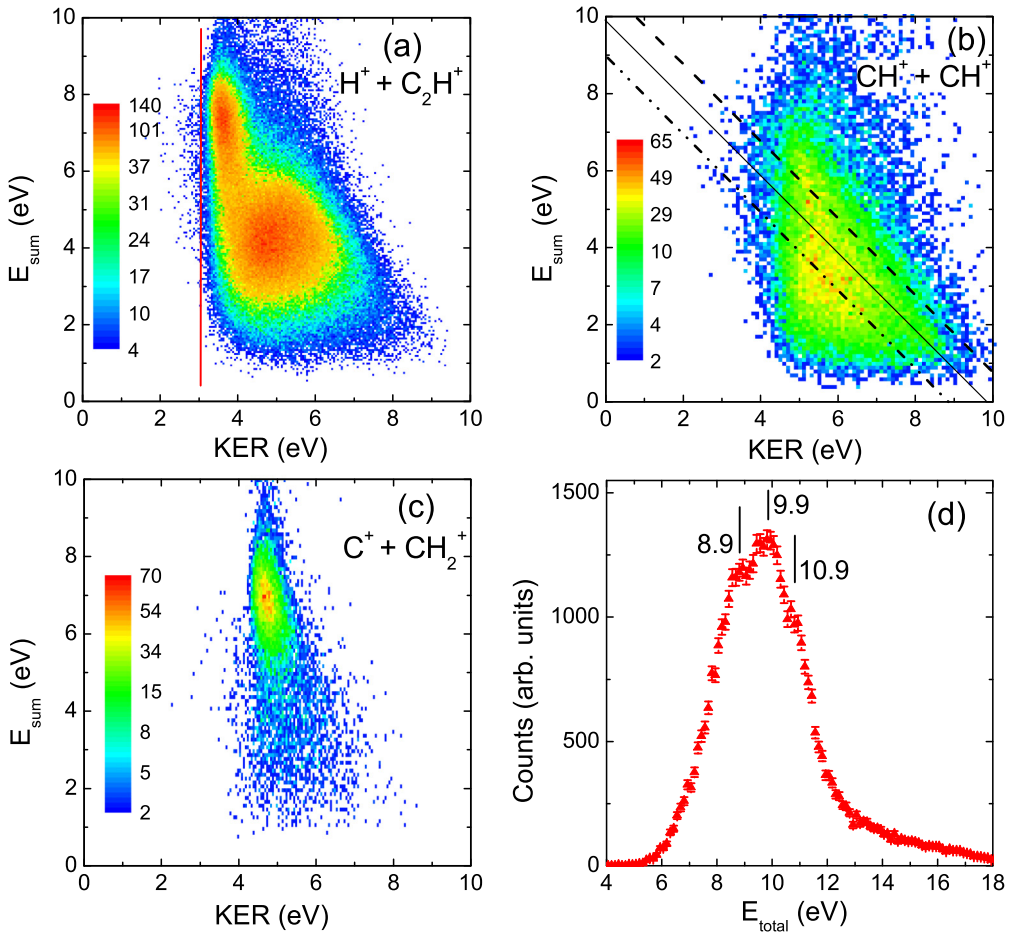

FIG. 9. (Color online) Energy correlation map of the KER along the horizontal axis and E_{sum} along the vertical axis for the (a) $H^+ + C_2H^+$, (b) $CH^+ + CH^+$, and (c) $C^+ + CH_2^+$ channels, respectively. The lines in (b) indicate three different possible pathways. The color scale is logarithmic with the same dynamic range for all the plots. (d) Total energy KER + E_{sum} distribution of the symmetric breakup channel displayed in (b).

Before we analyze each channel we give a general overview of the dissociation dynamics. The acetylene dication is comprised of several excited Π states that are conically intersected by the trio of fast dissociating $^1\Sigma_u^-$, $^3\Sigma_u^+$, and $^3\Delta_u$ states. The symmetric dissociation (C-C coordinate) with high E_{sum} is produced by one of these three states. The lower two Π states $^3\Pi_u$ and $^1\Pi_u$ dissociate directly to the deprotonation (C-H coordinate). The deprotonation at lower E_{sum} probably stems from a nonadiabatic coupling to the higher Π states. The high E_{sum} peak for the deprotonation likely results from a dissociation along the surfaces of lower-lying states.

TABLE V. Same as Table III but for the PDI of acetylene at 42-eV photon energy. We have estimated the absolute photoionization cross sections of these channels by normalizing to the total photoabsorption cross section of 8 Mb at 42-eV photon energy [65,66] and 0.01 Mb of the $C^+ + CH_2^+$ channel [11]. The absolute photoionization cross sections for the $C_2H_2^{2+}$, $H^+ + C_2H^+$, and $CH^+ + CH^+$ channels are 0.46, 0.25, and 0.04 Mb, respectively. Based on these numbers, the ratio of double to single ionization at a photon energy of 42 eV turns out to be 10%.

Channels	E_{sum}	E_{vert}	KER	States	Branching ratio (%)
$C_2H_2^{2+}$	8.8	33.2		$^3\Sigma_g^-$	60.4 ± 1.9
$H^+ + C_2H^+$	4.25	37.75	4.75	$^1\Pi_u$,$^3\Pi_u$	26.2 ± 0.9
	7.25	34.75	3.75	$^3\Sigma_g^-$	7.0 ± 0.2
$CH^+ + CH^+$	3	39	5	$^3\Sigma_g^-$,$^3\Pi_g$,$^1\Sigma_u^-$	5.0 ± 0.2
$C^+ + CH_2^+$	6.75	35.25	4.5	$^1\Sigma_g^+$	1.3 ± 0.1

1. NDI: $C_2H_2^{2+}$

The E_{sum} distribution of the electrons measured in coincidence with the metastable dications ($C_2H_2^{2+}$) from the NDI channel of acetylene has a peak at about $E_{\text{sum}} = 8.8$ eV, which suggests a 33.2-eV vertical energy for the double ionization. This value is in good agreement with previous measurements [15,16,68], as shown in Table VI. The likely states with the vertical energy of around 33 eV are the electronic ground state $^3\Sigma_g^-$ and the singlet $^1\Delta_g$ and $^1\Sigma_g^+$ states with the possibility of simultaneous vibrational excitation during the ionization. All of these states have quasibound potential wells (see Fig. 10). The $^3\Sigma_g^-$ state is favored over the other two singlet states based on the propensity rule (valence), which states that singlet ungerade and triplet gerade states of the dication are favored [5,30,31] in the photo-double-ionization

TABLE VI. Vertical DIPs for the electronic states of the acetylene dication at the geometry $R_{CC} = 2.2871$ bohrs and $R_{CH} = 2.0103$ bohrs. The column labeled "Prop" denotes whether or not the state is preferred by the propensity rule (double ionization preferentially populates singlet ungerade and triplet gerade states [5,30,31]). The "Channels" label denotes the dication breakup channels as (I) $H^+ + C_2H^+$, (II) $CH^+ + CH^+$, and (III) $C^+ + CH_2^+$, respectively. The state is check marked if it can dissociate directly and marked with an × if there is a likely dissociative pathway via a single conical intersection, to the indicated channel.

					Vertical DIP			
		Channels			Calculated			
State	Prop.	I	II	III	Present	Ref. [67]	Ref. [11]	Expt.
$^3\Sigma_g^-$	✓				31.98	31.35	32.0	31.7 [68] 32.7 [16]
$^1\Delta_g$					32.89	32.47	32.9	33.4 [15]
$^1\Sigma_g^+$				✓	33.57	33.24	33.5	
$^3\Pi_u$		✓	×		37.30	36.75	37.1	37.9 [16]
$^1\Pi_u$	✓	✓	×		38.08	37.64	37.8	
$^3\Pi_g$	✓		×		38.82	38.15	38.7	39.6 [16]
$^1\Sigma_u^-$	✓		✓		39.47		39.2	
$^3\Sigma_u^+$			✓		39.92		39.7	
$^3\Delta_u$			✓		40.21		39.5	

near threshold. The dication ground state corresponds to the electronic configuration $1\sigma_g^2 1\sigma_u^2 2\sigma_g^2 2\sigma_u^2 3\sigma_g^2 1\pi_u^2$, with two electrons removed from two different π orbitals [16].

The NDI is the dominant channel (with a branching ratio of 60.4%) in the PDI of acetylene near threshold, which is in contrast to the ethylene case (5.4% NDI only). The fact that the electronic ground state of $C_2H_2^{2+}$ is populated the most is also in accordance with the propensity rule (valence). However, in the ethylene dication case the electronic ground singlet state and the first triplet state are not favored by the propensity rule (valence).

2. *Deprotonation: $H^+ + C_2H^+$*

The energy correlation map of the deprotonation channel, shown in Fig. 9(a), has two distinct features. The major feature has KER and E_{sum} peaks at around 4.75 and 4.25 eV, respectively, while the minor feature has a KER peak around 3.75 eV and an E_{sum} peak around 7.25 eV. The KER values from this measurement are in good agreement with the values in the literature [9,11]. There are some extra features in our measured KER distributions compared to that of Ref. [9] due to a slightly higher photon energy that enables access to higher-lying excited states. For example, one can see two distinct peaks in the KER distribution of the deprotonation channel in Fig. 9(a). We are unaware of data in the literature with which to compare our E_{sum} values. However, the vertical energies can be compared to our previous measurement of the carbon K-shell ionization of acetylene followed by Auger decay [10] despite the drastically different photon energy and ionization mechanism. Many of the states identified in the present study (see Table V) are the same as those identified in Ref. [10]. However, in that paper only singlet states were considered because of the propensity rule (Auger) [37,38]. While this work is focused on the PDI of valence electrons, we consider both singlet and triplet states that are allowed to be populated by the propensity rule (valence).

The two distinct features in the deprotonation channel are the result of at least two different pathways. As shown below, one feature stems from the lower manifold of the electronic states and the other feature from the electronic excited states of the acetylene dication.

The feature with a broad KER distribution (peak around 4.75 eV) and an E_{sum} peak around 4.25 eV results from the states whose vertical energy is about 37.75 eV. The likely states are $^1\Pi_u$ and $^3\Pi_u$. Both of the states are dissociative in the C-H

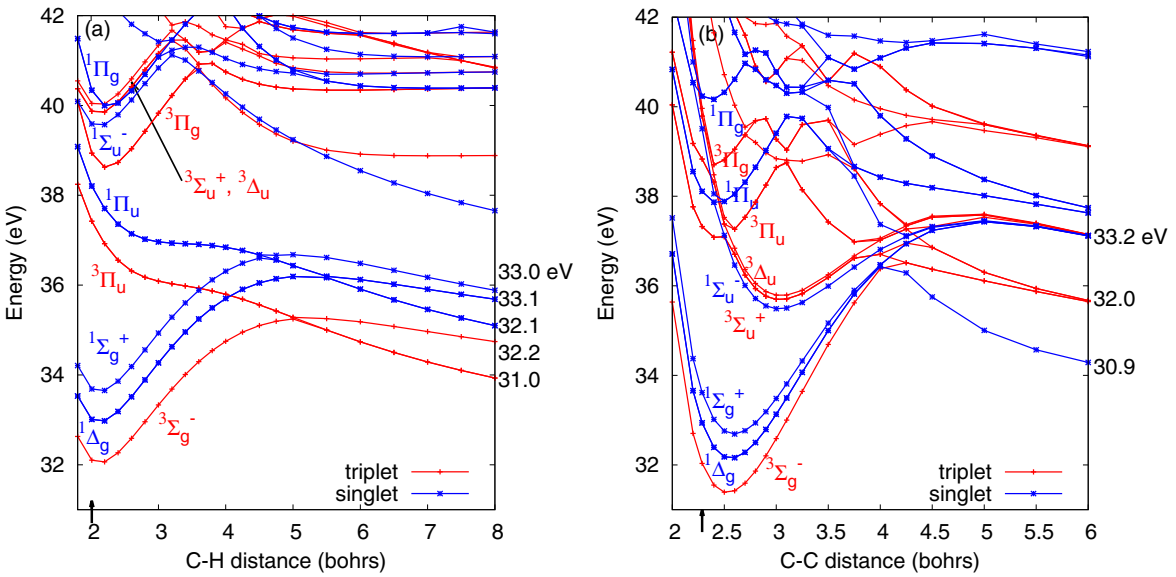

FIG. 10. (Color online) Cut of the potential energy surfaces (singlet and triplet states) of the acetylene dication for (a) C-H and (b) C-C distances calculated using the multiconfiguration self-consistent field method. The vertical arrows indicate the Franck-Condon region. States are labeled with the irreducible representations appropriate at the equilibrium geometry of the neutral molecule.

coordinate as shown in the cut of the PESs as a function of the C-H distance in Fig. 10(a). The dissociation along the surface of the $^1\Pi_u$ state results in a KER of 6.0 eV and the DI along the $^3\Pi_u$ state leads to a KER value of 6.3 eV. The propensity rule (valence) favors the $^1\Pi_u$ state.

The next feature in the deprotonation channel has KER and $E_{\rm sum}$ values of 3.75 and 7.25 eV, respectively. This feature has a narrower KER distribution than the other feature (described in the preceding paragraph). Based on the vertical energy of 34.75 eV, the likely pathway for this feature involves the lowest manifold of electronic states, namely, $^3\Sigma_g{}^-$, $^1\Delta_g$, and $^1\Sigma_g{}^+$, with possible vibrational excitation. By surveying the cuts of the PESs of these states along the C-H coordinate [shown in Fig. 10(a)], the barrier height of the $^3\Sigma_g{}^-$ state is about the same as the measured vertical energy. So the dications with sufficient energy to overcome the barrier dissociate. This manifests itself in the sharp cutoff on the lower-energy side of the KER distribution as seen in Fig. 9(a), marked with a vertical line around a KER of 3 eV for easier visualization.

The ground state has an asymptote calculated to be 31.0 eV. Taking 34.25 eV as the barrier height [14], one expects a KER of 3.25 eV at the onset, which agrees well with the present result of KER 3.75 eV. The barrier height of the other two singlet states $^1\Delta_g$ and $^1\Sigma_g{}^+$ in the C-H coordinate is higher than that of the triplet state $^3\Sigma_g{}^-$. Hence $^3\Sigma_g{}^-$ is the most likely state responsible for this feature.

3. Symmetric breakup: $CH^+ + CH^+$

In the case of the symmetric breakup (acetylene products) broad KER and $E_{\rm sum}$ distributions are observed in Fig. 9(b). The KER distribution extends from 4 to 8.5 eV with a peak at 5 eV. The $E_{\rm sum}$ distribution has a energy range from 1 to 7.5 eV with a peak at about 3 eV. This wide range of energy means that states with vertical energies from 41 to 34.5 eV are responsible for the symmetric breakup of acetylene.

Several excited states, namely, the $^1\Sigma_u{}^-$ (DIP of 39.47 eV), $^3\Sigma_u{}^+$ (DIP of 39.92 eV), and $^3\Delta_u$ (DIP of 40.21 eV), contribute to the lower $E_{\rm sum}$ feature. These states are fed through conical intersections with a manifold of Π states, specifically $^3\Pi_g$ (DIP of 38.82 eV), $^1\Pi_u$ (DIP of 38.08 eV), and $^3\Pi_u$ (DIP of 37.3 eV). These Π states are populated by the photoionization in the Franck-Condon region. The cut of the PESs of these states are shown in Fig. 10(b). The $^1\Sigma_u{}^-$, $^3\Sigma_u{}^+$, and $^3\Delta_u$ states also have quasibound potential wells (at around 3 bohrs) in a downhill dissociation path. When the dissociation begins at much higher energies in the Franck-Condon region, the barriers can be circumvented. There are three different asymptotic limits (with about 2.3-eV separation) at which the dissociation products may end up. This in turn results in a broad KER like the one that is measured.

For the higher $E_{\rm sum}$ value (say, 7.0 eV) the vertical energy is 35.0 eV and the states responsible for this feature are the lowest-lying states, i.e., $^3\Sigma_g{}^-$, $^1\Delta_g$, and $^1\Sigma_g{}^+$. The barriers to the symmetric breakup channels are around 34.56 [49] and 35.12 eV [14] for a bent geometry. However, the plots in Fig. 10(b) are for a linear geometry, where the barrier is much higher (approximately at 36 eV). The barrier clearly controls the maximum $E_{\rm sum}$ that is observed for the symmetric breakup channel. A typical dissociation involving a state with the asymptotic limit of 30.9 eV (Fig. 10) would thus result in a KER of 4.1 eV, which agrees well with our measured KER for the higher $E_{\rm sum}$ shown in Fig. 9(b).

The combination of all these pathways is expected to lead to a convoluted energy distribution like the one we have observed. The individual features associated with each pathway overlap. However, we see structure (marked with lines) in the energy correlation map shown in Fig. 9(b). One can see the individual features in the total energy (KER plus $E_{\rm sum}$) distribution of the symmetric channel displayed in Fig. 9(d). The peaks are about 1 eV apart from one another and so are the asymptotic limits of the lower-lying states in Fig. 10(b) that are responsible for this channel.

4. Vinylidene: $C^+ + CH_2{}^+$

The energy correlation map of the vinylidene channel ($C^+ + CH_2{}^+$) is shown in Fig. 9(c). One can see a distribution that peaks around a KER of 4.5 eV and $E_{\rm sum} = 6.8$ eV. The vertical energy of 35.2 eV indicates that the lowest manifold of states (namely, $^3\Sigma_g{}^-$, $^1\Delta_g$, and $^1\Sigma_g{}^+$) with vibrational excitation are responsible for the vinylidene channel. The vertical energy and KER are in agreement with the K-shell ionization measurements in Ref. [10]. This suggests that the same pathway, involving the $^1\Sigma_g{}^+$ state with 35.35-eV barrier height [10], is responsible for the vinylidene channel in the direct photo-double-ionization of acetylene.

5. Summary: Acetylene photo-double-ionization

The threshold energy plot, shown in Fig. 11, reveals that the NDI of acetylene involves the states with a vertical energy around 33 eV. At a slightly higher threshold energy of about 34.5 eV the vinylidene and the deprotonation channels open up. As we go further up in the threshold energy the major feature of the deprotonation and the symmetric breakup channels dominate over the NDI channel.

Among the DI channels of acetylene the deprotonation has the highest branching ratio (33.2%) as in the case of the PDI of ethylene. The vinylidene channel has the smallest branching ratio (1.3%) and the symmetric breakup channel branching

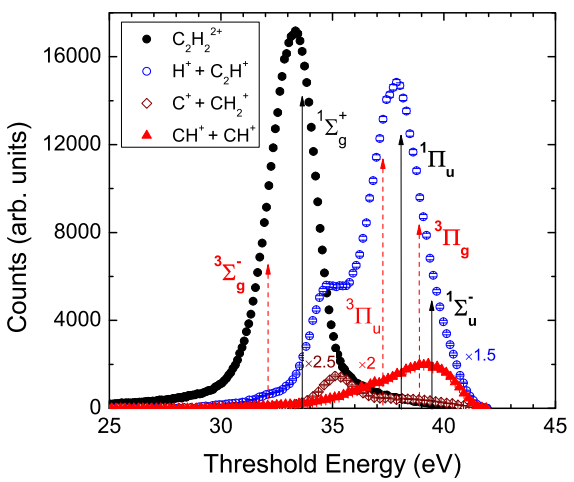

FIG. 11. (Color online) Same as Fig. 4 but for the PDI of acetylene using 42-eV photons (linearly polarized light).

ratio is about 5.0%. By looking at the PESs in Fig. 10, one can see that the PESs in the C-H coordinate have smaller barriers than in the C-C coordinate and hence breaking the C-H bond, leading to a deprotonation, is more likely than breaking the C≡C bond. Since the ground state $^3\Sigma_g{}^-$ can be populated by the propensity rule (valence) and also has a deep potential well, the NDI channel is the dominant channel (60.4%) in the PDI of acetylene.

V. SUMMARY

In conclusion, we have presented kinematically complete measurements of the direct photo-double-ionization of ethylene and acetylene molecules near threshold. With our COLTRIMS setup we are able to identify both nondissociative and dissociative double ionization of these molecules. In accordance with the propensity rule (valence), suggested decades ago, and the barrier to torsion around the C-C bond, our results clearly show that the electronic ground state of the ethylene dication is hardly populated. The likelihood of removing the two π electrons from the outermost occupied orbital, which is responsible for restricting the torsion of the ethylene molecule, by direct PDI must be very small. The same scenario applies to the PDI of acetylene molecules where the electronic ground state of the dication (a triplet state $^3\Sigma_g{}^-$) is a product of removing two electrons from different orbitals. The measured branching ratio of the NDI channel is higher in acetylene.

Our theoretical results allow us to unravel the states for the NDI channel and the dissociation dynamics for the DI channels. We have found that the electronic excited states of the ethylene dication contribute mainly to the DI channels and very little to the NDI channel. We have also found that the first excited singlet state contributes directly to the deprotonation channel and indirectly to the symmetric channel via the ultrafast population transfer through the conical intersection to the electronic ground state S_1. Both processes are interesting candidates for time-resolved studies employing pump-probe techniques. We theorize that the passage through the conical intersection will produce interesting effects on the electron angular distributions. On another note, our observation of similar yields of metastable ethylene dications produced by PDI of valence electrons or Auger decay via K-shell ionization is intriguing and warrants further theoretical investigation.

ACKNOWLEDGMENTS

This work was supported by the Director, Office of Science, Office of Basic Energy Sciences and by the Division of Chemical Sciences, Geosciences, and Biosciences of the US Department of Energy at LBNL under Contract No. DE-AC02-05CH11231. W.C., M.Z., C.L.C., and I.B. were supported by Grant No. DE-FG02-86ER13491 from the same funding agency. We acknowledge financial support from the DAAD and the DFG. We thank the staff of the Advanced Light Source, in particular A. Aguilar and D. Kilcoyne from beamline 10.0.1, for their outstanding support. This article is based upon work partially supported by the US Government under the DOE. The views and opinions of the authors expressed herein do not necessarily state or reflect those of the US Government or any agency thereof. The US Government is authorized to reproduce and distribute reprints for governmental purposes.

[1] T. Weber, A. O. Czasch, O. Jagutzki, A. K. Müller, V. Mergel, A. Kheifets, E. Rotenberg, G. Meigs, M. H. Prior, S. Daveau *et al.*, Nature (London) **431**, 437 (2004).
[2] M. Gisselbrecht, M. Lavollée, A. Huetz, P. Bolognesi, L. Avaldi, D. P. Seccombe, and T. J. Reddish, Phys. Rev. Lett. **96**, 153002 (2006).
[3] R. Dörner, H. Bräuning, J. M. Feagin, V. Mergel, O. Jagutzki, L. Spielberger, T. Vogt, H. Khemliche, M. H. Prior, J. Ullrich *et al.*, Phys. Rev. A **57**, 1074 (1998).
[4] P. Lablanquie, J. Mazeau, L. Andric, P. Selles, and A. Huetz, Phys. Rev. Lett. **74**, 2192 (1995).
[5] S. Hsieh and J. H. D. Eland, J. Phys. B **29**, 5795 (1996).
[6] E. Ohrendorf, H. Köppel, L. S. Cederbaum, F. Tarantelli, and A. Sgamellotti, J. Chem. Phys. **91**, 1734 (1989).
[7] C. Benoit and J. A. Horsley, Mol. Phys. **30**, 557 (1975).
[8] K. Lammertsma, M. Barzaghi, G. A. Olah, J. A. Pople, A. J. Kos, and P. v. R. Schleyer, J. Am. Chem. Soc. **105**, 5252 (1983).
[9] M. Alagia, C. Callegari, P. Candori, S. Falcinelli, F. Pirani, R. Richter, S. Stranges, and F. Vecchiocattivi, J. Chem. Phys. **136**, 204302 (2012).
[10] T. Osipov, T. N. Rescigno, T. Weber, S. Miyabe, T. Jahnke, A. S. Alnaser, M. P. Hertlein, O. Jagutzki, L. P. H. Schmidt, M. Schöffler *et al.*, J. Phys. B **41**, 091001 (2008).
[11] R. Thissen, J. Delwiche, J. M. Robbe, O. Duflot, J. P. Flament, and J. H. D. Eland, J. Chem. Phys. **99**, 6590 (1993).
[12] T. Osipov, C. L. Cocke, M. H. Prior, A. Landers, T. Weber, O. Jagutzki, L. Schmidt, H. Schmidt-Böcking, and R. Dörner, Phys. Rev. Lett. **90**, 233002 (2003).
[13] R. Flammini, E. Fainelli, F. Maracci, and L. Avaldi, Phys. Rev. A **77**, 044701 (2008).
[14] T. S. Zyubina, Y. A. Dyakov, S. H. Lin, A. D. Bandrauk, and A. M. Mebel, J. Chem. Phys. **123**, 134320 (2005).
[15] O. Furuhashi, T. Kinugawa, S. Masuda, C. Yamada, and S. Ohtani, Chem. Phys. Lett. **342**, 625 (2001).
[16] S. Andrews, F. Harris, and D. Parry, Chem. Phys. **166**, 69 (1992).
[17] J. Appell, J. Durup, F. C. Fehsenfeld, and P. Fournier, J. Phys. B **7**, 406 (1974).
[18] P. G. Fournier, J. Fournier, M. L. Langford, and F. M. Harris, Chem. Phys. **178**, 581 (1993).
[19] R. Cooks, T. Ast, and J. H. Beynon, Int. J. Mass Spectrom. Ion Phys. **11**, 490 (1973).
[20] M. Rabrenovic and J. H. Beynon, Int. J. Mass Spectrom. Ion Process. **54**, 79 (1983).
[21] R. R. Rye, T. E. Madey, J. E. Houston, and P. H. Holloway, J. Chem. Phys. **69**, 1504 (1978).
[22] M. Thompson, P. A. Hewitt, and D. S. Wooliscroft, Anal. Chem. **48**, 1336 (1976).

[23] P. M. Guyon, J. Mentall, I. Nenner, N. Moulin, and R. Botter, Adv. Mass Spectrom. **7A**, 188 (1978).

[24] T. Ibuki, G. Cooper, and C. E. Brion, Chem. Phys. **129**, 295 (1989).

[25] T. Ibuki, T. Imamura, I. Koyano, T. Masuoka, and C. E. Brion, J. Chem. Phys. **98**, 2908 (1993).

[26] J. Ullrich, R. Moshammer, A. Dorn, R. Dörner, L. P. H. Schmidt, and H. Schmidt-Böcking, Rep. Prog. Phys. **66**, 1463 (2003).

[27] S. Lee, Ph.D. thesis, University of California Davis, 2009.

[28] M. Lundqvist, D. Edvardsson, P. Baltzer, and B. Wannberg, J. Phys. B **29**, 1489 (1996).

[29] E. V. Doktorov, I. Malkin, and V. I. Man'ko, J. Mol. Spectrosc. **56**, 1 (1975).

[30] J. H. D. Eland, S. D. Price, J. C. Cheney, P. Lablanquie, I. Nenner, and P. G. Fournier, Philos. Trans. R. Soc. London Ser. A **324**, 247 (1988).

[31] P. Lablanquie, J. H. D. Eland, I. Nenner, P. Morin, J. Delwiche, and M. J. Hubin-Franskin, Phys. Rev. Lett. **58**, 992 (1987).

[32] G. H. Wannier, Phys. Rev. **90**, 817 (1953).

[33] A. Temkin, Phys. Rev. Lett. **49**, 365 (1982).

[34] A. Knapp, M. Walter, T. Weber, A. L. Landers, S. Schössler, T. Jahnke, M. Schöffler, J. Nickles, S. Kammer, O. Jagutzki *et al.*, J. Phys. B **35**, L521 (2002).

[35] H. Bräuning, R. Dörner, C. L. Cocke, M. H. Prior, B. Krässig, A. Bräuning-Demian, K. Carnes, S. Dreuil, V. Mergel, P. Richard *et al.*, J. Phys. B **30**, L649 (1997).

[36] T. Weber, A. Czasch, O. Jagutzki, A. Müller, V. Mergel, A. Kheifets, J. Feagin, E. Rotenberg, G. Meigs, M. H. Prior *et al.*, Phys. Rev. Lett. **92**, 163001 (2004).

[37] H. Ågren and O. Vahtras, J. Phys. B **26**, 913 (1993).

[38] T. Kerkau and V. Schmidt, J. Phys. B **34**, 839 (2001).

[39] H. Lischka, R. Shepard, I. Shavitt, R. M. Pitzer, M. Dallos, T. Müller, P. G. Szalay, F. B. Brown, R. Ahlrichs, H. J. Böhm *et al.*, COLUMBUS, an *ab initio* electronic structure program, release 7.0 (2012).

[40] R. Shepard, I. Shavitt, R. M. Pitzer, D. C. Comeau, M. Pepper, H. Lischka, P. G. Szalay, R. Ahlrichs, F. B. Brown, and J. Zhao, Int. J. Quantum Chem. Quantum Chem. Symp. **34**, 149 (1988).

[41] H. Lischka, R. Shepard, F. B. Brown, and I. Shavitt, Int. J. Quantum Chem. Quantum Chem. Symp. **15**, 91 (1981).

[42] H. Lischka, T. Müller, P. G. Szalay, I. Shavitt, R. M. Pitzer, and R. Shepard, WIREs **1**, 191 (2011).

[43] H. Lischka, R. Shepard, R. M. Pitzer, I. Shavitt, M. Dallos, T. Müller, P. G. Szalay, M. Seth, G. S. Kedziora, S. Yabushita *et al.*, Phys. Chem. Chem. Phys. **3**, 664 (2001).

[44] J. T. H. Dunning, J. Chem. Phys. **90**, 1007 (1989).

[45] M. J. Dewar and C. H. Reynolds, J. Mol. Struct. Theochem **136**, 209 (1986).

[46] R. H. Nobes, M. W. Wong, and L. Radom, Chem. Phys. Lett. **136**, 299 (1987).

[47] M. W. Wong, B. F. Yates, R. H. Nobes, and L. Radom, J. Am. Chem. Soc. **109**, 3181 (1987).

[48] W. J. Griffiths and F. M. Harris, Int. J. Mass Spectrom. Ion Process. **122**, 321 (1992).

[49] D. Duflot, J.-M. Robbe, and J.-P. Flament, J. Chem. Phys. **102**, 355 (1995).

[50] X. Li and H. B. Schlegel, J. Phys. Chem. A **108**, 468 (2004).

[51] G. Dujardin, S. Leach, O. Dutuit, P.-M. Guyon, and M. Richard-Viard, Chem. Phys. **88**, 339 (1984).

[52] D. M. Curtis and J. H. D. Eland, Int. J. Mass Spectrom. Ion Process. **63**, 241 (1985).

[53] J. H. D. Eland, F. S. Wort, and R. N. Royds, J. Electron Spectrosc. Relat. Phenom. **41**, 297 (1986).

[54] T. Osipov, M. Stener, A. Belkacem, M. Schöffler, T. Weber, L. Schmidt, A. Landers, M. H. Prior, R. Dörner, and C. L. Cocke, Phys. Rev. A **81**, 033429 (2010).

[55] D. R. Yarkony, Rev. Mod. Phys. **68**, 985 (1996).

[56] F. A. Grimm, Chem. Phys. **81**, 315 (1983).

[57] G. Cooper, T. N. Olney, and C. E. Brion, Chem. Phys. **194**, 175 (1995).

[58] D. A. Hagan and J. H. D. Eland, Org. Mass Spectrom. **27**, 855 (1992).

[59] J. Palaudoux, L. Jutier, and M. Hochlaf, J. Chem. Phys. **132**, 194301 (2010).

[60] B. Kempgens, H. M. Köppe, A. Kivimäki, M. Neeb, K. Maier, U. Hergenhahn, and A. M. Bradshaw, Phys. Rev. Lett. **79**, 35 (1997).

[61] L. J. Medhurst, T. A. Ferrett, P. A. Heimann, D. W. Lindle, S. H. Liu, and D. A. Shirley, J. Chem. Phys. **89**, 6096 (1988).

[62] A. L. D. Kilcoyne, M. Schmidbauer, A. Koch, K. J. Randall, and J. Feldhaus, J. Chem. Phys. **98**, 6735 (1993).

[63] B. Kempgens, A. Kivimäki, B. S. Itchkawitz, H. M. Köppe, M. Schmidbauer, M. Neeb, K. Maier, J. Feldhaus, and A. M. Bradshaw, J. Electron Spectrosc. Relat. Phenom. **93**, 39 (1998).

[64] M. N. Piancastelli, W. C. Stolte, G. Öhrwall, S.-W. Yu, D. Bull, K. Lantz, A. S. Schlachter, and D. W. Lindle, J. Chem. Phys. **117**, 8264 (2002).

[65] G. Cooper, T. Ibuki, Y. IIda, and C. E. Brion, Chem. Phys. **125**, 307 (1988).

[66] G. Cooper, G. R. Burton, and C. E. Brion, J. Electron Spectrosc. Relat. Phenom. **73**, 139 (1995).

[67] E. M.-L. Ohrendorf, F. Tarantelli, and L. S. Cederbaum, J. Chem. Phys. **92**, 2984 (1990).

[68] J. R. Appling, B. E. Jones, L. E. Abbey, D. E. Bostwick, and T. F. Moran, J. Org. Mass Spectrom. **18**, 282 (1983).